CrystEngComm

Accepted Manuscript

ROYAL SOCIETY OF CHEMISTRY

www.rsc.org/crystengcomm

Journal Name

PAPER

Large Scale Fabrication of Dumbbell-shaped Biomimetic SiC/SiO_2 Fibers

Received 00th January 20xx,
Accepted 00th January 20xx

DOI: 10.1039/x0xx00000x

www.rsc.org/

Wenna Liu[a], Junhong Chen[b], Kuo-Chih Chou[a] and Xinmei Hou[a*]

Abstract. The mechanical property of dumbbell fibers-reinforced composite is expected to be improved via enhancing the interface adhesion between the matrix and the fibers from the viewpoint of biomimetics. In the present work, the mass production of dumbbell-shaped biomimetic SiC/SiO_2 fibers via a facile carbothermal reduction method using gangue and carbon black as raw material at 1500℃ in argon is reported. The phase and morphology of the obtained fibers were characterized using XRD, XPS, FTIR, FESEM and HRTEM techniques. It is found that the string of the synthesized biomimetic fibers is single-crystal 3C-SiC with diameter of 0.5-1μm and the beads are amorphous SiO_2 with diameter of about 5 μm. The effect of holding time at 1300℃ on the morphology is further investigated. Based on these, the growth mechanism of dumbbell-shaped biomimetic SiC/SiO_2 fibers is proposed.

1. Introduction

The toughened ceramic-matrix composites (CMCs) exhibit high toughness in addition to the desirable properties of monolithic ceramics such as high strength, good hardness, wear resistance, excellent corrosion, thermal shock and oxidation resistance by promoting crack bridging [1, 2], crack deflection [3] and pull-out mechanisms [4, 5]. SiC fibers have demonstrated as good candidates as reinforcements in a variety of CMCs owing to their outstanding properties such as excellent oxidative stability, high strength, high thermal stability and good chemical inertness [6–12]. A variety of methods have been applied to prepare SiC fibers [13-16]. Among these, the carbothermal reduction process is considered to be a promising method due to efficiency and economy [17-20].

The intrinsic properties of CMCs are determined by their structure, especially the structure of the reinforced phase, i.e. size, shape, composition and crystallinity [21, 22]. Many techniques have recently been developed to shape nanoscale materials as tubes, wires, belts, disk, cubes, and branched structures [23-27]. Saito et al. [28] produced SiC whiskers from SiO(g)-CO(g) system. They investigated the effects of the partial pressure of SiO and CO and the deposition temperature on the morphology. From the mechanical viewpoint, the advantage of the dumbbell-shaped or chain-like fibers is that the enlarged end allows load to be effectively transferred from the matrix to the reinforcing fibers instead of relying on an overly strong fiber/matrix interface [29, 30]. At the same time, SiO_2 bead around the core could act as excellent blockades to prevent SiC fibers withdrawing from the surrounding matrix [31]. Therefore the dumbbell-shaped fibers as reinforced phase in CMCs are expected. Hou et al. [32] and Wei et al. [33] produced SiC/SiOx nanochain heterojunctions via pyrolysis of polymeric precursors and microwave method respectively. No further work is reported up to now.

In present research, the mass production of dumbbell-shaped biomimetic SiC/SiO_2 fibers via a facile carbothermal reduction method was reported. To our best knowledge, this rout allows us to prepare dumbbell-shaped biomimetic SiC/SiO_2 fibers in gram yields which have not been reported up to now.

2. Experimental

2.1 Material preparation

Gangue (SiO_2 > 99%) and carbon black were used as silicon and carbon sources respectively. The mixture ball-mixed with the mole ratio of 1:3 was put in a ceramic boat and placed in the hot zone of the furnace equipped with carbon as the inner lining. Before heating, the furnace was vacuumed and introduced argon (99.9%; CO_2: 7.8 ppm; O_2: 9.3 ppm; H_2O: 12.5 ppm) at a constant gas flow rate of 0.4 L/min. The total gas pressure is kept at about 0.12 MPa. Then the samples were heated up to the desired temperature of 1500℃ with a heating rate of 3℃/min and holding for 2 h. After that, the furnace was cooled to 1300℃ and kept for 0.5 h. Finally the furnace was cooled to ambient temperature, argon was stopped and large scale gray-white fibers were obtained mainly on the top of the furnace.

[a] W. N. Liu • T. Yang • Kuo-Chih Chou • X. M. Hou (corresponding author)
State Key Laboratory of Advanced Metallurgy, University of Science and Technology Beijing, Beijing 100083, China
E-mail: houxinmei@ustb.edu.cn

[b] J. H. Chen (corresponding author)
School of materials engineering, University of Science and Technology Beijing, Beijing 100083, China.
E-mail: chenjunhong2666@126.com

2.2 Phase and microstructure characterization

The phases were identified by X-ray diffraction (XRD) using Cu Kα radiation (40KV, 20mA, λ=1.5406 Å) in the angular 10-80° with the scan speed of 2°/min. Raman spectra were carried out on a ALMEGA confocal laser micro-Raman spectrometer using Arion laser excitation with a wavelength of 532 nm. Morphologies of the products were examined by a field emission scanning electron microscope (SEM) operated at 20 kV (FEI-SIRION). Transmission electron microscopy with high-resolution transmission electron microscopy (HRTEM) and selected area electron diffraction (SAED) were performed on a Tecnai G2 F30 S-TWIN. Fourier transformation infrared (FT-IR) spectra in transmission mode were recorded on a Nicolet-Nexus 470 infrared spectrophotometer with a spectral scanning range 2000-400 cm^{-1}. The chemical states of Si were determined by X-ray photoelectron spectroscopy (XPS) in a VG Multilab 2009 system with a monochromatic Mg Kα source and a charge neutralizer.

3. Results and discussion

Figure 1a shows the XRD pattern of the obtained sample. As can be seen from the pattern, the major peaks at 2θ = 35.8 °, 41.4 °, 60.0 °, 71.8 ° and 75.6°can be indexed as the (111), (200), (220), (311) and (222) reflections of 3C-SiC. A broad amorphous peak at 15°-30° also appears which corresponds to the amorphous state SiO_2. The lattice constant is calculated to be 4.361 A, which is close to the standard value of 3C-SiC˚ (a = 4.359 A) (JCPDS, no. 29-1129), indicating 3C-SiC is successfully synthesized. The samples were also investigated using Raman spectroscopy. The Raman spectrum shown in Fig. 1b confirms the fibers as SiC. The peak around 795 cm^{-1} is attributed to the transverse optical (TO) mode of 3C-SiC while the peak center at 970 cm^{-1} is the characteristic of the longitudinal optic (LO) phonon mode. This two Raman peaks are shifted by a few wavenumbers to lower frequencies than that of bulk material (TO mode at 796 cm^{-1} and LO mode at 972 cm^{-1}) [34], which may be caused by the structure defaults in the fibers. Also, we can see another peak at 942 cm^{-1} which is attributed to SiO_2. The Si 2p fine XPS spectrum of the SiC/SiO_2 is presented in Fig. 1c. In the spectrum of Si 2p, the peak centered at 100.5 eV corresponds to the Si–C bond in SiC [35] and the peak at 102.5 eV and 103.4eV can be assigned to Si-O bond [36, 37].

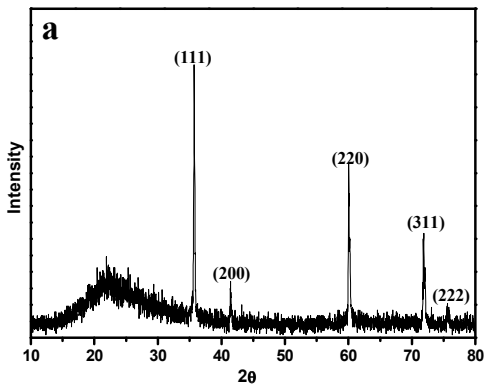

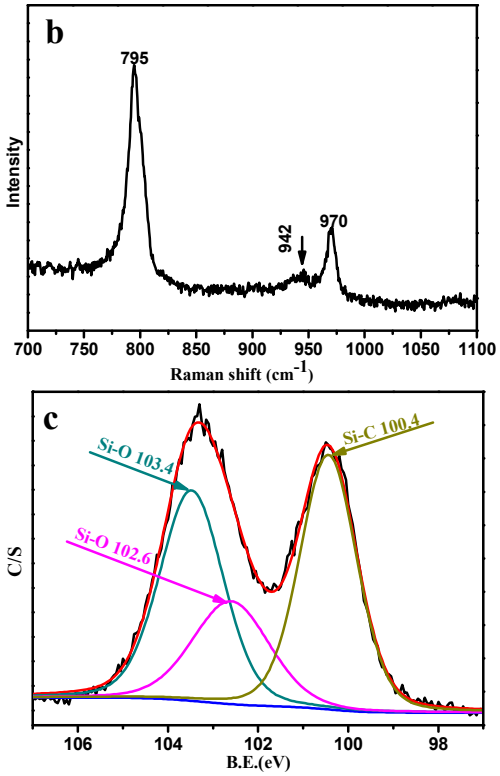

Fig.1 (a) XRD pattern, (b) Raman spectrum, (c) XPS spectrum of the synthesized fibers.

The morphology of the synthesized fibers was characterized using SEM. It can be seen that high density fibers were synthesized with the length ranging from several to tens of microns (Fig. 2a), and the insert is a photo of the large scale product. At high magnification, the representative dumbbell-shaped fiber is presented (Fig. 2b), which is distinctively different from the conventional fibers. The beads on each individual string have a uniform size and were separated evenly. The chemical compositions of the fibers string (A in Fig. 2b) and bead (B in Fig. 2b) were analyzed using EDS under SEM as shown in Fig. 2c and Fig. 2d respectively. The string consists of Si, C and O elements (Fig. 2c) while the beads are composed of Si and O elements (Fig. 2d), revealing that the beads should be SiO_2 and the string be SiC as well as SiO_2. From the element mapping of the sample shown in Figs. 2(e-g), element O predominately distributes at the beads (Fig. 2e) while Si element exists uniformly in all area (Fig. 2f). Considering C element is too light, the C mapping has little reference value (Fig. 2g). Fig. 2h is an optical microscope image of the typical dumbbell-shaped biomimetic SiC/SiO_2 fiber. The photo shows a central wire decorated with regularly spaced beads along their length. In order to further verify the string-bead-shape structure and the composition of the beads, the fibers were etched in hydrogen fluoride (HF) solution (20%) for 10 and 20 min as shown in Fig. 2i, Fig. 2j respectively considering SiC cannot be etched in hydrogen fluoride (HF) while SiO_2 can be easily etched away. When etched for 10 min, the beads were destroyed and loose (Fig. 2i). While the beads disappeared completely and only string was left behind when etched for 20 min (Fig. 2j). EDS analysis of the fibers etched for 20 min in the Fig. 2k

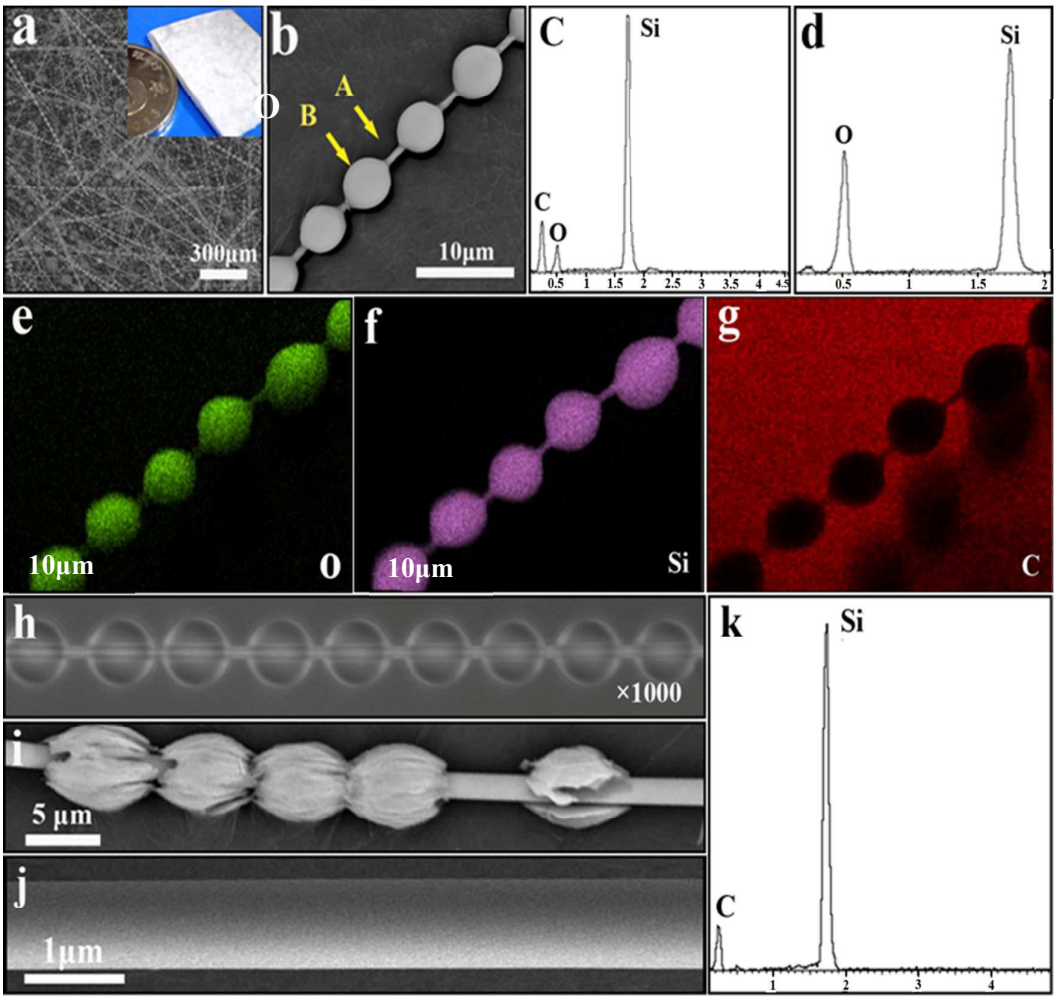

Fig. 2. (a) low-magnification SEM image of the product, the insert is a photo shows the large scale product, (b) high magnification SEM images of a single fiber, (c, d) EDS spectrums of the string (A in fig. 2b) and bead (B in fig. 2b), (e-g) the mapping of O, Si, C in the fiber respectively, (h) photo of a typical dumbbell-shaped biomimetic fiber magnified 1000 times, (i) and (j) SEM images of the fiber etched by HF solution for 10 min and 20 min respectively, (k) EDS spectrum of the fibers etched for 20min.

indicates only the phase of SiC was left. From above results, the fabricated products possess a typical bead–string structure and the bead is the amorphous SiO_2.

Fig. 3a is a typical TEM image of the obtained structures under low magnification. The closer observations of the rod (Fig. 3b) reveal that the products are actually structured with a dark SiC core and a light SiO_2 shell. The SiC core has identical diameters of about 500 nm while the bead was 5 μm in diameter. Fig. 3c is a typical HRTEM image recorded from the marked area in Fig. 3b. The d-space of the two sets of fringes are measured to be 0.25 nm, which corresponds to the (111) plane of 3C-SiC. The inset in Fig. 3c is the typical selected area electron diffraction (SAED) pattern corresponding to the string, indicating the core of the fiber is single crystal 3C-SiC. The HRTEM analysis provides further insight into the structure of the bead-string-shape. Both the SAED patterns and the HRTEM image suggest that the SiC fibers grow along the [111] direction.

To investigate the possible formation process of the dumbbell shape SiC fibers, the products obtained under different soaking time at 1300℃ were checked. The experimental process is all same except that the time kept at 1300℃ became 10, 20 min respectively. Fig. 4shows the corresponding SEM images. When the soaking time is 10min, some of the string–bead structures occurred with small SiO_2 attached SiC string as indicated with an arrow in Fig. 4a. When the time increased to 20 min, the bead is gradually formed with an ellipsoidal shape (Fig. 4b). It is worth noting that the beads are changed from the ellipsoidal shapes to spheroidal ones when the time increased to 30 min (Fig. 4c). Fig. 4d is the low magnification image of the products reacted for 30 min. For the most part, the observed beads possess almost perfectly spherical shapes and smooth surfaces due to minimize the free energy [31]. From above results, the bead is formed in the cooling stage and the bead shapes can be tunable by the soaking time. This is in agreement with Ref. [33]

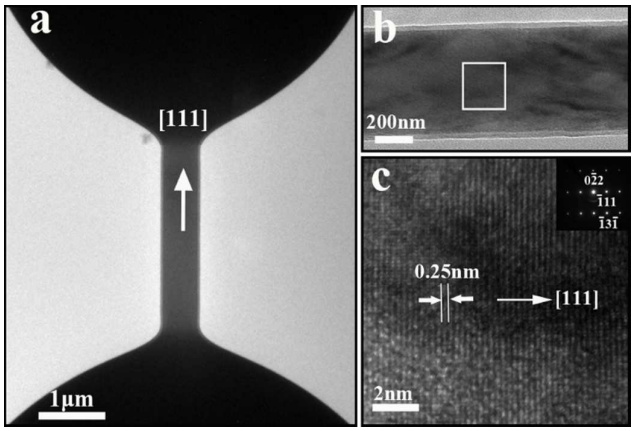

Fig. 3. (a)Typical TEM image of the dumbbell-shaped biomimetic SiC/SiO_2 fibers, (b)closer observation of the string, (c) HRTEM image of the selected area in (b) and the insert is the corresponding SAED pattern,

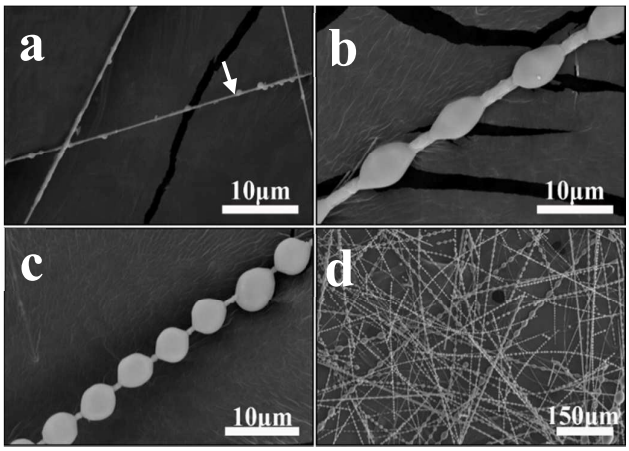

Fig. 4. The SEM images of fibers holding different time at 1300℃. (a)10 min, (b) 20 min, (c) and (d) 30 min

In view of the growth mechanism of dumbbell-shaped biomimetic SiC/SiO_2 fibers, there are generally two kinds of growth mechanisms proposed for the formation of heterogenous nanostructures. One is the formation of inner 1D core structures and then the epitaxial growth of secondary branches [38-40]. The other is the self-assembly of nanobuilding blocks, such as platelets, into hierarchical structures [41]. In our experiment, the SiC/SiO_2 fibers are typical bead–string structure as shown in Fig.2h. It should belong to a two-step epitaxial process, i.e. vapor -solid (VS) mechanism followed by modulation process. The process is schematically shown in Fig. 5.

(1) the growth of SiC fibers (I). It could be performed by VS mechanism, which has been reported in detail in our recent work [42]. Three main reactions involved during the synthesis process are illustrated below:

$$SiO_2(s)+C(s) \rightarrow SiO(g) + CO(g) \quad (1)$$

$$SiO(g)+3CO(g) \rightarrow SiC(s)+ 2CO_2(g) \quad (2)$$

$$C(s)+CO_2(g) \rightarrow 2CO(g) \quad (3)$$

In our experiment, SiO and CO vapours were produced at 1500 ℃ through Eqs. (1-3) and SiC fibers grow along the [111] direction on the graphite substrates through VS mechanism by Eq. (2).

(2) Modulation step. When the temperature decreased to 1300℃, the saturated vapour pressures of SiO decreases and this contributed to the formation of SiO_2 by following equations.

$$SiO(g)+O_2(g) \rightarrow SiO_2(s) \quad (4)$$

$$SiO(g)+H_2O(g) \rightarrow SiO_2(s)+H_2(g) \quad (5)$$

$$SiO(g)+CO_2(g) \rightarrow SiO_2(s)+CO(g) \quad (6)$$

CO_2, O_2 and H_2O originated from the argon (CO_2: 7.8 ppm; O_2: 9.3 ppm; and H_2O: 12.5 ppm). With time prolonging, more and more SiO transformed into SiO_2 to formed SiO_2 layer on the surface of SiC fibers. Because of the Rayleigh instability and the poor wettability between SiC and SiO_2, SiO_2 is separated into spheres and forms the first batch of SiO_2 beads (III in Fig.5) [31, 43]. It deserves to be mentioned that there is enough SiO_2 is formed in this experiment due to the above reaction. Therefore dumbbell-shaped biomimetic SiC/SiO_2 fibers are formed.

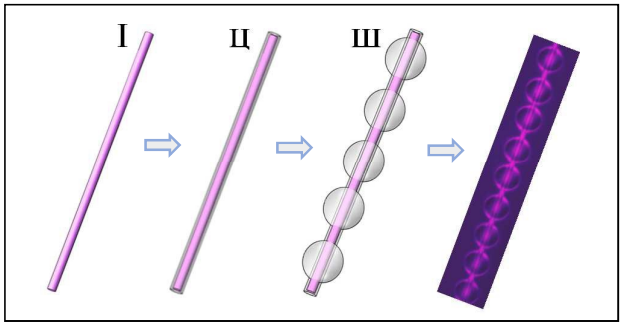

Fig. 5. schematic illustration of the dumbbell-shaped biomimetic SiC/SiO_2 fiber.

Conclusions

A facile strategy for the mass production of dumbbell-shaped biomimetic SiC/SiO_2 fibers via carbothermal reduction method is reported. SiC/SiO_2 fibers are composed of single-crystalline 3C-SiC string cores growing along the [111] direction and amorphous periodic SiO_2 bead shells. Two-step growth mechanism, i.e. VS following by modulation is applied to explain the growth process of dumbbell-shaped biomimetic SiC/SiO_2 fibers. The size of amorphous periodic SiO_2 beads can be tailored by controlling the holding time at 1300℃. Due to the fascinating structures, SiC/SiO_2 fibers can be a promising candidate as reinforcement in CMCs.

Acknowledgements

The authors express their appreciation to National Nature Science Foundation of China (No. 51174022, 51474141 and 51572019). The authors also appreciate the National Science Fund for Excellecnt Young Scholars of China (No. 51522402) for financial support.

Notes and references

1 B. Budinansky and J. Amazigo, J. Mech. Phys. Solids, 1989 **37**, 93–109.
2 P.F. Becher, J. Am. Ceram. Soc. 1991, **74**, 255–269.
3 K.T. Faber and A.G. Evans, Acta. Metallurgica 1983, **31**, 565-576.
4 Y.P. Xie, L.F. Cheng, L.J. Li, H. Mei and L.T. Zhang, J. Eur. Ceram. Soc., 2013, **33**, 1701–1706.
5 Q.F. Zan, L.M. Dong, C. Wang, C.A. Wang and Y. Huang, Ceram. Int., 2007, **33**, 385–388.
6 D. Zhu, M.X. Gao, H.G. Pan, Z.L. Hong, B.Y. Zhao, S.Q. Li and H.W. Ge. Int. J. Refract. Met. H, 2012, **35**, 152–158.
7 O. Chakrabarti, L. Weisensel and H. Sieber, J. Am. Ceram. Soc., 2005, **88**, 1792– 1798.
8 W. Yang, H. Araki, C.C. Tang, S. Thaveethavorn, A. Kohyama and H. Suzuki, Adv. Mater., 2005, **17**, 1519–1523.
9 W. Yang, H. Araki, S. Thaveethavorn, H. Suzuki and T. Noda. J. Am. Ceram. Soc., 2004, **87**, 1720–1725.
10 S.M. Kang, W.J. Kim, S.G. Yoon and J.Y. Park. J. Nucl. Mater. 2011, **417**, 367–370.
11 D. Zhu, M.X. Gao, S.C. Zhang, H.Y. Wu, Y. Pan and Y.F. Liu, J. Mater. Sci., 2012, **47**, 4921–4927.
12 N. Jiraborvornpongsa, M. Imai, K. Yoshida and T. Yano. J. Mater. Sci., 2013, **48**, 7022–7027.
13 Y. Sun, H. Cui, G.Z. Yang, H. Huang, D. Jiang and C.X. Wang, CrystEngComm., 2010, **12**, 1134-1138.
14 J.X. Dai, J.J. Sha, Z.F. Zhang, Y.C. Wang and W, Krenkel. Ceram. Int., 2015, **41**, 9637-9641.
15 H. Cui, Y. Sun, G.Z. Yang, J. Chen, D. Jiang and C.X. Wang. Chem. Commun. 2009, **41**, 6243-6245.
16 S.C. Chiu, C.W. Huang and Y.Y. Li. J. Phys. Chem. C, 2007, **111**, 10294-10297.
17 M. Taghavi, E. Ghasemi and A. Monshic, J. Ceram. Process Res. 2014, **15**, 242-245.
18 R. Dhiman, E. Johnson and P. Morgen, Ceram. Int. 2011, **37**, 3759-3764
19 Z. Li, T.J. Shi and D.X. Tan, J. Am. Ceram. Soc., 2010 **93**, 3499-3503.
20 J.S. Lee, S.H. Lee, T. Nishimura and H.J. Tanaka, Am. Ceram. Soc. 2009, **92**, 1030-1035.
21 R.E. Smalley and B.I. Yakobson, SolidStateCommun. 1998, **107**, 597-606.
22 L. Manna, D.J. Milliron, A. Meisel, E.C. Scher and A.P. Alivisatos, Nature mater., 2003, **2**, 382-385.
23 S. Iijima and T. Ichihashi, Nature, 1993, **363**, 603-605.
24 T.M. Whitney, P.C. Searson, J.S. Jiang and C.L. Chien. Science, 1993, **261**, 1316-1319.
25 Z.W. Pan, Z.R. Dai and Z.L. Wang. Science, 2001, **291**, 1947-1949.
26 C. Pacholski, A. Kornowski and H. Weller, Angew. Chem. Int. Edit., 2002, **41**, 188-1191.
27 G. Shen, Y. Bando and D. Golberg, Cryst. Growth Des. 2007, **7**, 35-38.
28 M. Saito, S. Nagashima and A. Kato, J. Mater. Sci. Lett. 1992, **11**, 373-376.
29 X.K. Sun, R.S. Qin, D.M. Liu and B.L. Zhou, Acta. Metallurgica Sinica. 1997, **33**, 781-784
30 X. Tao, J. Liu, G. Koley and X. Li. Adv. Mater., 2008, **20**, 4091-4096.
31 M. Bechelany, J.L. Riesterer, A. Brioude, D. Cornu and P. Miele. CrystEngComm. 2012, **14**, 7744-7748.
32 H. Hou, L. Wang, F. Gao, G. Wei, J. Zheng and X. Cheng, CrystEngComm. 2013, **15**, 2986-2991.
33 G. Wei, W. Qin, K. Zheng, D. Zhang, J. Sun, J. Lin and L. Wang, Cryst. Growth Des. 2009, **9**, 1431-1435.
34 S. Nakashima and H. Harima, Phys. Status Solidi (a) 1997, **162**, 39–64.
35 Y. Mizokawa, K.M. Geib and C.W. Wilmsen, J. Vac. Sci. Technol. A, 1986, **4**, 1696-1700
36 Q. Li, C.A. Wang and S. Tie. Cryst. Res. Technol. 2014, **49**, 290-297.
37 F. Rueda, J. Mendialdua, A. Rodriguez, R. Casanova, Y. Barbaux, L. Gengembre and L. Jalowiecki. J. Electron Spectrosc. 1996, **82**, 135-143.
38 W. Lu, Y. Ding, Y. Chen, Z.L. Wang and J. Fang, J. Am. Chem. Soc. 2005,**127**, 10112-10116.
39 Y.C. Zhu, Y. Bando and LW Yin, Adv. Mater. 2004, **16**, 331-334.
40 M. Bechelany, A. Brioude, P. Stadelmann, G. Ferro, D. Cornu, P. Miele, Adv. Funct. Mater. 2007, **17**, 3251-3257.
41 L.W. Yin, Y. Bando, Y.C. Zhu, M.S. Li, Y.B. Li and D. Golberg, Adv. Mater. 2005, **17**, 110-114.
42 J.H. Chen, W.N. Liu, T. Yang, B. Li, J.D. Su, X.M. Hou, K.C. Chou. Cryst. Growth Des. 2014, **14**, 4624-4630.
43 M. Bechelany, X. Maeder, J. Riesterer, J. Hankache, D. Lerose and S. Christiansen, Cryst. Growth Des. 2010, **10**, 587-596.
44 Z. Pan, S. Dai, D.B. Beach and D.H. Lowndes, Nano Letters, 2003, **3**, 1279-1284.